Materials Today Physics 30 (2023) 100960

Contents lists available at ScienceDirect

Materials Today Physics

journal homepage: www.journals.elsevier.com/materials-today-physics

Predicted THz-wave absorption properties observed in all-inorganic perovskite $CsPbI_3$ thin films: Integrity at the grain boundary

Inhee Maeng [a,1], Shi Chen [b,1], Seungjun Lee [c,1,2], Shenghao Wang [b,*], Young-Kyun Kwon [c,d,**], Min-Cherl Jung [e,***]

[a] YUHS-KRIBB, Medical Convergence Research Institute, College of Medicine, Yonsei University, Seoul, 03722, Republic of Korea
[b] Materials Genome Institute, Shanghai University, Shanghai, 200444, China
[c] Department of Physics, Kyung Hee University, Seoul, 02447, Republic of Korea
[d] Department of Information Display and Research Institute for Basic Sciences, Kyung Hee University, Seoul, 02447, Republic of Korea
[e] Division of Materials Science, Faculty of Pure and Applied Sciences, University of Tsukuba, Ibaraki, 305-8577, Japan

ARTICLE INFO

Keywords:
All-inorganic perovskite thin film
γ-$CsPbI_3$
Clean grain boundary
THz-wave absorption
Three major THz absorptions

ABSTRACT

The realization of terahertz (THz) detectors using organic-inorganic hybrid perovskite (OHP) materials presents a challenge because of the high real conductivities and broad THz absorption spectra required. The control of phonon vibration modes in OHPs depends on the control of defect states such as the defect-incorporated perovskite structure and the δ/α-mixed interfacial structure observed in $MAPbI_3$ and δ/α-mixed $FAPbI_3$, respectively. Difficulties with defect control in particular materials may amplify relative risk factors and invite strong resistance to commercialization. As an alternative to OHPs, the all-inorganic perovskite material $CsPbI_3$ (lacking the hydrophobic organic cations that generate structural defects) constitutes a good candidate for THz detectors. We investigated the phonon vibration modes of thin films of the all-inorganic perovskite γ-$CsPbI_3$ containing no atomic or chemical defect states. We observed the three expected major phonon vibration modes at 0.9, 1.5, and 1.8 THz that originate from the transverse I–Pb–I frame, the Cs–I–Cs optical vibration, and the longitudinal I–Pb–I frame, respectively, finding good agreement with theoretical simulations. Significantly, the real conductivity of these all-inorganic perovskite thin films ranged from approximately 10–40 S/cm across a broad frequency range of 0.5–3.0 THz, demonstrating the material's considerable potential for application as a THz-band detector.

1. Introduction

The investigation of terahertz (THz)-based applications using organic-inorganic hybrid perovskite (OHP) materials has received considerable attention recently, founded on an understanding of the origins of phonon vibration modes among organic cations, metal cations, and halogen anions [1–6]. Initial expectations were that OHP materials would accommodate phonon energies in the required range of 0.5–3.0 THz by virtue of their perovskite structures' lattice vibrations (in the 1–100 THz range) and their molecular libration/rotation frequencies (0.3 and 2 THz, respectively). Additionally, these materials demonstrated strong potential as THz detectors [7–13]. Sensitive room temperature detection of THz is still challenging constrained by the THz photon energy which is lower than the thermal energy of room temperature. Several 2D materials including graphene, $MoS_{2.19}$, Bi_2Te_3 and black phosphorous, are successfully demonstrated as a room temperature THz detector but these devices are required complicated fabrication methods such as defect engineering, heterojunction or homojunction structure of 2D material and antenna coupling to improve their performance [14,15]. Perovskite materials can be used to THz detector by itself using the photothermoelectric effect [16,17].

The practical realization of THz detectors using OHP thin films

* Corresponding author.
** Corresponding author. Department of Physics, Kyung Hee University, Seoul, 02447, Republic of Korea.
*** Corresponding author.
E-mail addresses: shenghaowang@shu.edu.cn (S. Wang), ykkwon@khu.ac.kr (Y.-K. Kwon), jung.mincherl.fp@u.tsukuba.ac.jp (M.-C. Jung).
[1] These authors contributed equally: Inhee Maeng, Shi Chen, and Seungjun Lee.
[2] Present address: Department of Electrical and Computer Engineering, University of Minnesota, Minneapolis, Minnesota 55455, USA.

https://doi.org/10.1016/j.mtphys.2022.100960
Received 5 October 2022; Received in revised form 23 November 2022; Accepted 26 December 2022
Available online 29 December 2022

demands easy fabrication, material stability, high real conductivity, and a broad absorption spectrum [1,2]. A primary requirement for device realization is the control of structural defect states in OHP thin films, such as $MAPbI_3$ and δ/α-mixed $FAPbI_3$ hybrid perovskites, originating from molecular defect-incorporated perovskite structures and unusual interfacial phonon vibrations, respectively [2–5]. The absence of effective defect control can generate a level of relative risk that becomes a major obstacle to commercial application. In order to overcome the difficulties associated with defect control, all-inorganic perovskite materials such as cesium lead iodide ($CsPbI_3$) have been proposed as promising candidates for THz detectors [18]. These materials lack the hydrophobic organic cations that cause structural defects in OHP materials because of the effects of moisture, oxygen, UV light, and heat. No substantial investigation of the THz absorption properties of all-inorganic perovskite thin films has yet been published.

In solar-cell applications using all-inorganic perovskite materials, significant power conversion efficiencies as high as 19.03% have been detected [19]. However, $CsPbI_3$ thin films have critical issues, such as rapid structural degradation from α, β, and γ-phase to δ-phase structures, inhomogeneous film morphology, and high surface defect density [20]. These findings pose challenges to the application of $CsPbI_3$ thin films as THz detectors. These challenges may be mitigated by preparing a well-organized thin film without defect structures in the grains or in the grain boundaries to confirm the THz absorption properties of the material [21,22].

In this study, we fabricated γ-$CsPbI_3$ thin films at different post-annealing temperatures while changing annealing times to acquire a variety of grain sizes. We applied basic characterization methods to confirm the defect states in the atomic and chemical structures. No defect states were observed. We observed THz absorption occurring over a wide frequency range (0.5–3.0 THz) and with high real conductivity (~40 S/cm at 1.8 THz) without any dependence on the grain size in the formed γ-$CsPbI_3$ thin films, which is consistent with our theoretical calculations. Additionally, we also observed strong THz absorption after structural degradation from the γ-to the δ-phase. (For details on δ-$CsPbI_3$, see Appendix A).

2. Material and methods

Materials used in our experiments include PbI_2 (99.99%, Xi'an Polymer Light Technology, Xi'an, China), CsI (99.99%, Alfa Aesar), *N*,*N*-dimethylformamide (DMF; 99.8%, Sigma-Aldrich), hydrogen iodide (57%, Aladdin Industrial Corporation), ethanol (AR, General-Reagent), chlorobenzene (CB; 99.8%, Sigma-Aldrich), and poly[bis(4-phenyl)(2,4,6-trimethylphenyl)amine] (PTAA, MN17000; Xi'an Polymer Light Technology). The materials were used as received, without any purification. $DMAPbI_3$ crystals (DMA^+ = dimethylammonium, $(CH_3)_2NH_2^+$) were prepared by dissolving 6.915 g of PbI_2 and 5.4 ml hydroiodic acid in 15 ml DMF to form a mixed solution. The solution was heated at 120 °C in a chlorobenzene vapor environment in the air for 10 h. The solvent was evaporated, and chlorobenzene was diffused into the solution to reduce the solubility of $DMAPbI_3$. Needle-like crystals of $DMAPbI_3$ gradually appeared. The needle-like crystals were washed several times with ethanol to remove the residual solvent. Finally, the $DMAPbI_3$ crystals were dried at 70 °C in a vacuum oven for 24 h.

The sapphire and high-doped Si(100) substrates were cleaned sequentially with deionized water and acetone by ultrasonication for 10 min. Subsequently, the substrates were rinsed in heated acetone for 1 min and treated with UV-ozone for 30 min. The $CsPbI_3$ precursor was prepared by dissolving 0.9 mmol $DMAPbI_3$ and 0.9 mmol CsI in 1 ml DMF, and then stirred at 60 °C for 12 h. The $CsPbI_3$ films were fabricated by spin-coating the precursor solution on the substrates at 3000 rpm for 30 s and then annealing at 180 °C for 12 min (A), 195 °C for 8 min (B), and 210 °C for 4 min (C), respectively, to form three samples with different grain sizes. Finally, the PTAA layer (using a 1.25 mg/ml concentration in CB) was deposited on the formed films by spin-coating at 2000 rpm for 1 min [1,2].

We performed basic characterizations such as X-ray diffraction (XRD), scanning electron microscopy (SEM), and X-ray photoelectron spectroscopy (XPS) to confirm the atomic structure, surface morphology, and chemical states of the prepared films. XRD patterns were obtained using a diffractometer (D2 PHASER Desktop XRD, Bruker, Billerica, MA, USA) with Cu Kα radiation. The UV–visible absorption spectra were measured using a spectrometer (Lambda 750; PerkinElmer, Waltham, MA, USA). The morphologies were characterized using SEM (FEI Helios G4 UC, Thermo Fisher Scientific, Waltham, MA, USA). XPS was performed using a PHOIBOS 150 analyzer (SPECS, Berlin, Germany) with monochromatic Al Kα (1486.6 eV) radiation as the X-ray source.

We employed terahertz time-domain spectroscopy (THz-TDS) to characterize the phonon modes of the γ- and δ-$CsPbI_3$ thin films in the range from 0.2 to 3 THz. We used a typical THz-TDS system based on a femtosecond (fs) laser which employs an 800 nm central wavelength Ti: sapphire (Tsunami, Spectra-physics, Milpitas, CA, USA) using an 80 fs pulse-width. THz pulses were generated on the surface of a *p*-InAs wafer via transient current and detected via photoconductive antenna sampling [23]. The generated THz pulses were focused on the sample using TPX lenses, and the THz path was covered and filled with dry air to eliminate water vapor absorption.

The transmitted THz signals through the sample $E_{sample}(t)$ B and the sapphire substrate reference $E_{reference}(t)$ are taken in the time domain and converted into frequency domain by fast Fourier transformation Fig. S1 (a, b). The transmission spectra $|\widetilde{T}(\omega)|$ is shown in Fig. S1(c). One measurement lasted 30 min, with no degradation observed in the samples with the PTAA protective layer. No significant absorption of the THz-wave on the PTAA film was observed [1,2]. (Fig. S1(d)).

3. Theoretical calculations

To understand the underlying physics of the observed THz absorption of γ- and δ-$CsPbI_3$, we performed first-principles calculations based on density functional theory [24], as implemented in the Vienna *ab initio* simulation package (VASP) [25,26]. We used projector-augmented wave pseudopotentials [27,28] to describe the valence electrons and employed the revised Perdew-Burke-Ernzerhof exchange-correlation functional for solids [29]. The wave functions were expanded on a plane-wave basis with a kinetic energy cutoff of 500 eV, and the Brillouin zone was sampled using $9 \times 9 \times 7$ and $9 \times 5 \times 2$ k-point meshes for γ- and δ-$CsPbI_3$, respectively.

The phonon dispersion relations were calculated using the finite displacement method [30]. We used $2 \times 2 \times 2$ and $3 \times 2 \times 1$ supercell structures for γ- and δ-$CsPbI_3$, respectively, and the corresponding reduced Brillouin zone was sampled only at the Γ point. The THz absorption spectra were calculated using the THz absorption intensity $I_{\mathrm{THz}}(\nu)$, which is defined as [31].

$$I_{THz}(\nu) \propto \sum_{i=1}^{3} \left| \sum_{n=1}^{N} \sum_{j=1}^{3} Z_{ij}^{*} \frac{u_{nj}(\nu)}{\sqrt{m_n}} \right|^2, \quad (1)$$

where ν is the phonon mode index, Z_{ij}^{*} is the Born effective charge tensor, N is the total number of atoms, m_n is the mass of the nth atom, and i and j denote the Cartesian coordinates. A Lorentzian convolution with a width of 5 THz was used to resemble a realistic frequency dependence.

4. Results and discussion

We performed XRD measurements to confirm the atomic structures of the formed samples under different annealing conditions (A, B, and C) and observed only the clear γ-phase in all the samples [19,32] (Fig. 1a). None of the samples contained any other atomic phase. The formed samples showed clear grains on the surface with a dark black color, which made it difficult to distinguish each sample (Fig. 1b–d). We

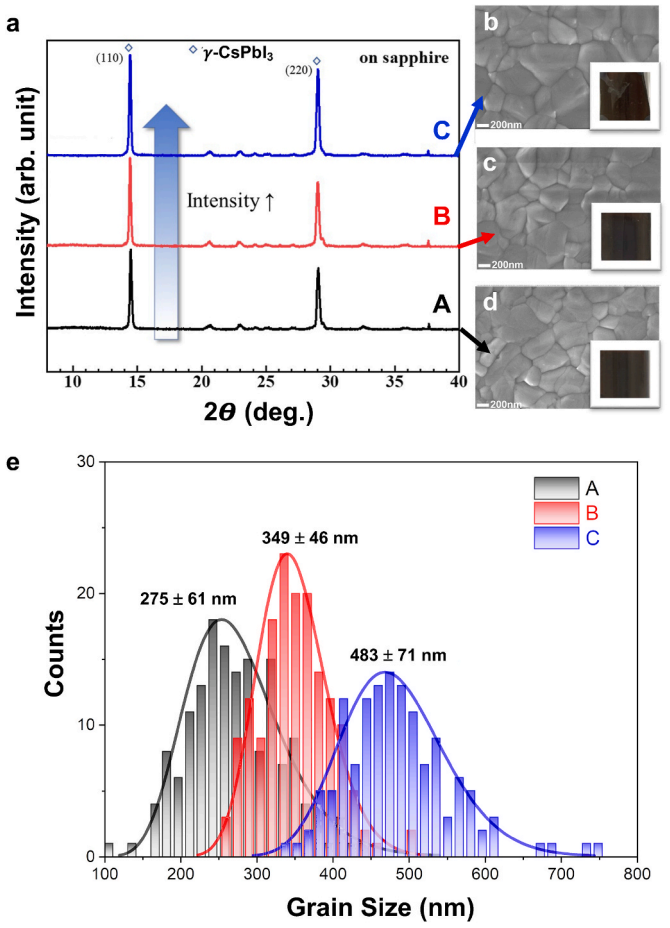

Fig. 1. **a** XRD results and surface morphologies for each different annealing condition **b-d**. SEM photographs of grains. **e** Distributions of grain sizes. The grain size in each treatment is increased from 300 to 450 nm in average. All samples were confirmed to contain only the γ-phase.

calculated the grain sizes in all the samples and confirmed average grain sizes of 275 ± 61 nm, 349 ± 46 nm, and 483 ± 71 nm for samples A, B, and C, respectively (Fig. 1e). The average grain sizes of samples A and B differed by approximately 70 nm, and those of samples B and C differed by approximately 130 nm.

The optical measurements obtained with the UV–Vis spectrometer indicated the same optical bandgap of 1.72 eV for all the samples [19,32] (Fig. 2a). Furthermore, we confirmed that no defect state was indicated by the XPS measurements in any of the core-level spectra (such as Cs 3*d*, Pb 4*f*, and I 3*d*) (Fig. 2b–d). Although we observed small peaks in the C 1*s*, N 1*s*, and O 1*s* core-level spectra (Fig. S2), there were no significant chemical bonds to Cs, Pb, or I (Fig. 2b–d). We attributed the small peaks of C, N, and O to physisorption on the surface during the sample transfer from the glovebox to the vacuum chamber for the XPS measurement.

We confirmed two important results through the basic characterization. First, the thin films that were formed displayed a single crystal-like atomic phase. Second, there were no atomic/chemical defects in the grains or their boundaries. This resulted in different formation behaviors compared to $MAPbI_3$ and δ/α-mixed $FAPbI_3$ hybrid perovskite thin films [1,2]. The organic-inorganic hybrid perovskite thin films, such as $MAPbI_3$ and δ/α-mixed $FAPbI_3$, exhibit significant phonon vibration modes originating from the defect-incorporated perovskite structure and from two different phase interfaces, respectively [1,2]. In previous reports, the atomic and chemical states at the grain boundaries were the primary factors controlling the phonon vibration modes of the structures. However, for the all-inorganic perovskite thin films consisting of γ-$CsPbI_3$, we did not observe any structural defects that induced defect-incorporated phonon modes in the measurement ranges of XRD, UV–Vis., and XPS [1,5,33,34]. Consequently, the phonon vibration modes of γ-$CsPbI_3$ can be predicted on the basis of their excellent match with simulations.

To observe the phonon vibration modes of γ-$CsPbI_3$, we performed THz-TDS, which delivered accurate complex conductivities that enabled the exploration of the rotational and vibrational resonance of the molecules [1,2,5,33]. We obtained time-domain THz spectra transmitted through the γ-$CsPbI_3$ perovskite film on the substrate for the THz-TDS analysis. In addition, a fast Fourier transformation yielded the magnitude and phase difference of the complex transmission amplitude of the sample. The real THz conductivities of the films were extracted using an analytical formula including multiple reflections [35,36] (Fig. 3a).

$$\tilde{T}(\omega)=\frac{E_{sample}(\omega)}{E_{reference}(\omega)}=\frac{2\tilde{n}(\tilde{n}_{sub}+1)}{(1+\tilde{n})(\tilde{n}+\tilde{n}_{sub})}\bullet exp\left[\frac{-i(\tilde{n}-1)\omega L}{c}\right]\bullet FP(\omega) \quad (2)$$

with

$$FP(\omega)=\frac{1}{1-\left(\frac{\tilde{n}-1}{\tilde{n}+1}\right)\left(\frac{\tilde{n}-\tilde{n}_{sub}}{\tilde{n}+\tilde{n}_{sub}}\right)\bullet exp\left[-\frac{2i\omega L\tilde{n}}{c}\right]}$$

where $\tilde{n}$ is the refractive index of the perovskite film, $\tilde{n}_{sub}$ is the refractive index of the sapphire substrate, L is the film thickness, c is the speed of light in vacuum. $FP(\omega)$ is the Fabry-Perot effect term which is presented the summation of multiple reflections. THz conductivity $\tilde{\sigma}(\omega)$ are converted by the relation of $\tilde{\sigma}(\omega)=i\omega\varepsilon_0(1-\tilde{n}^2)$.

The obtained conductivity spectrum was fitted with the Lorentz harmonic oscillator (LHO) model (Equation (2)) to gain insight into the phonon absorption behavior [36]:

$$\tilde{\sigma}(\omega)=-i\varepsilon_0\omega(\varepsilon_\infty-1)+\sum_j\frac{\varepsilon_0\Omega_j^2\omega}{i\left(\omega_{0j}^2-\omega^2\right)+\omega\gamma_j} \quad (3)$$

where ω_{0j}, Ω_j, and γ_j are the resonance frequency, oscillator strength, and scattering rate, respectively, of the jth oscillator. The peaks at the real conductivities appeared at the resonant frequencies of the phonon modes. However, in this case, it was difficult to evaluate the conductivity spectrum quantitatively without employing a fitting procedure because the absorption peaks were broadened and overlapped. We used three main Lorentzian oscillators and two minor oscillators to fit samples A, B, and C. (The resonance frequencies, oscillator strengths, and scattering rates derived from samples A, B, and C are summarized in Table S1.) We confirmed that the correlations between the resonance frequencies and oscillator strengths were similar for all the samples, for a variety of grain sizes. (Fig. 3b) The real conductivities of samples A, B, and C and the contributions of the individual Lorentzian oscillators are plotted in Fig. 3c–e. Three strong absorption peaks are observed near 0.9, 1.5, and 1.8 THz in all three γ-$CsPbI_3$ samples (A, B, and C) without any obvious dependence on grain size. This result is consistent with our assumption in the basic characterizations, and it confirms the different formation behavior of γ-$CsPbI_3$ in comparison with $MAPbI_3$ and δ/α-$FAPbI_3$ hybrid perovskite thin films.

Furthermore, the self-degradation of γ-$CsPbI_3$ into δ-$CsPbI_3$ is well established [32]. We confirmed this self-degradation in our samples without the PTAA protection layer and repeated the XRD experiment [32] (Fig. S3). δ-$CsPbI_3$ and PbI_2 were observed in all the samples (Fig. S3). We confirmed the absence of THz-wave absorption of PbI_2 which was stated in our previous reports [2,3,5,33,34]. THz-TDS measurements were repeated with the degraded samples in the δ-phase (Fig. S4). The structural phase transition from γ-$CsPbI_3$ to δ-$CsPbI_3$ directly influenced the real conductivity of THz radiation. The positions of the main peaks of δ-$CsPbI_3$ at 0.9, 1.4, and 1.8 THz in the real conductivities were similar to those of γ-$CsPbI_3$ (Fig. 3 and S4). However, the conductivity spectrum of δ-$CsPbI_3$ appeared much sharper,

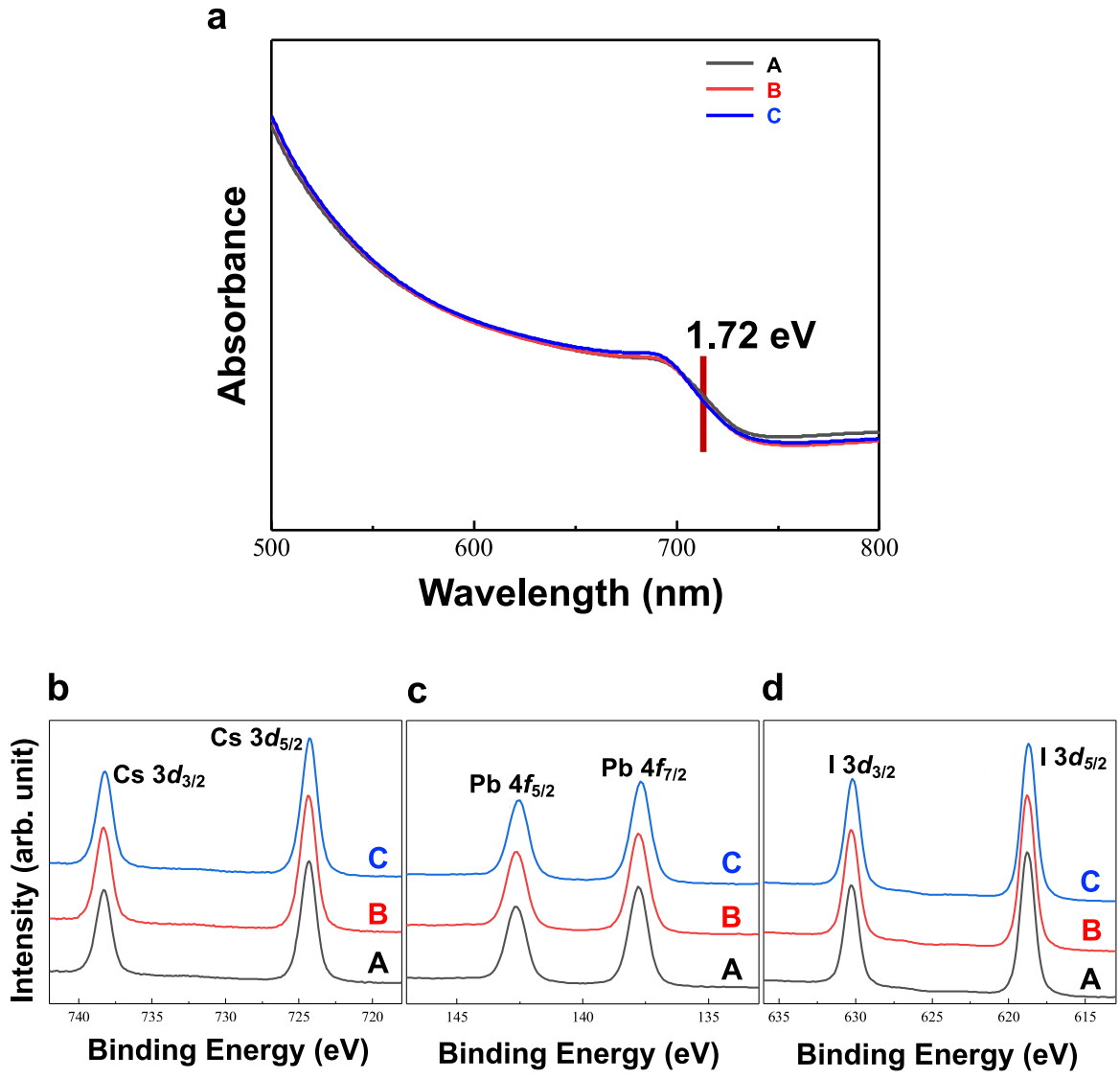

Fig. 2. The measurements of **a** optical band gap and chemical states of **b** Cs 3*d*, **c** Pb 4*f*, **d** I 3*d* using UV–Visible spectrometer and XPS, respectively. No evidence of atomic or chemical defect states is visible.

rendering the resonant frequency immediately recognizable (Fig. S4a). The strengths of the minor peaks at 2.1 and 2.7 THz were substantially enhanced to values comparable with those of the main peaks, and an additional peak emerged at 2.5 THz (Fig. S4b-d). Further details about the Lorentzian parameters for δ-$CsPbI_3$ appear in Appendix A (Table S2).

To understand the origin of the strong THz absorption of γ-$CsPbI_3$, we performed first-principles calculations based on density functional theory. Our experimental observations unambiguously revealed consistent THz absorption spectra regardless of the grain size of γ-$CsPbI_3$, implying that there were no strong interface- or defect-related phonon vibrations in our samples. A direct inference is that the observed strong THz absorption probably originated from the bulk phonon vibrations of $CsPbI_3$. To validate our hypothesis, we investigated the phonon properties of the bulk γ-$CsPbI_3$. The equilibrium lattice constants of γ-$CsPbI_3$ were calculated as $a = 8.366$ Å, $b = 8.952$ Å, and $c = 12.392$ Å, which were in good agreement with previous reports [37]. Based on this structure, we calculated the phonon dispersion relation using the finite displacement (FD) method, as shown in Fig. 4a. Although the FD method often fails to describe the room-temperature phases of organic-inorganic hybrid perovskites [1,2], we obtained a clear phonon dispersion relation without any imaginary phonon modes, which confirms that the FD method is an appropriate approach for describing the vibrational properties of γ-$CsPbI_3$.

The THz absorption spectrum of γ-$CsPbI_3$ was calculated, based on the calculated phonon band structures combined with the material's Born effective charge tensors, as shown in Fig. 4b. The overall shape of the calculated absorption spectrum was very similar to that of the experimentally measured spectrum. Furthermore, the calculated absorption peaks near 0.7, 1.6–1.8, and 2.0 THz can be associated with the experimentally observed peaks at 0.9, 1.5, and 1.8 THz. Therefore, we confirmed that the observed THz absorption spectrum originated purely from γ-$CsPbI_3$. For a more concrete understanding, we also investigated real-space vibrations of the corresponding absorption peaks at 0.72, 1.76, and 2.03 THz, as shown in Fig. 4c–e. We found that the first and third peaks approximately corresponded to the transverse and longitudinal optical vibration modes of the I–Pb–I frames, whereas the Cs–I–Cs optical vibration along the in-plane direction (along *a* or *b* lattice vectors) led to the second peak. Moreover, the asymmetrical crystal structure of γ-$CsPbI_3$ leads to complicated extra vibration modes near these three main phonon modes. For example, the absorption peak near 1.6 THz corresponds to the Cs–I–Cs optical vibration along the out-of-plane direction (along the *c* lattice vector), which has a lower vibration frequency than its in-plane counterpart. Therefore, the broad THz spectra observed in the experiments are not only typical of thermal or non-ideal

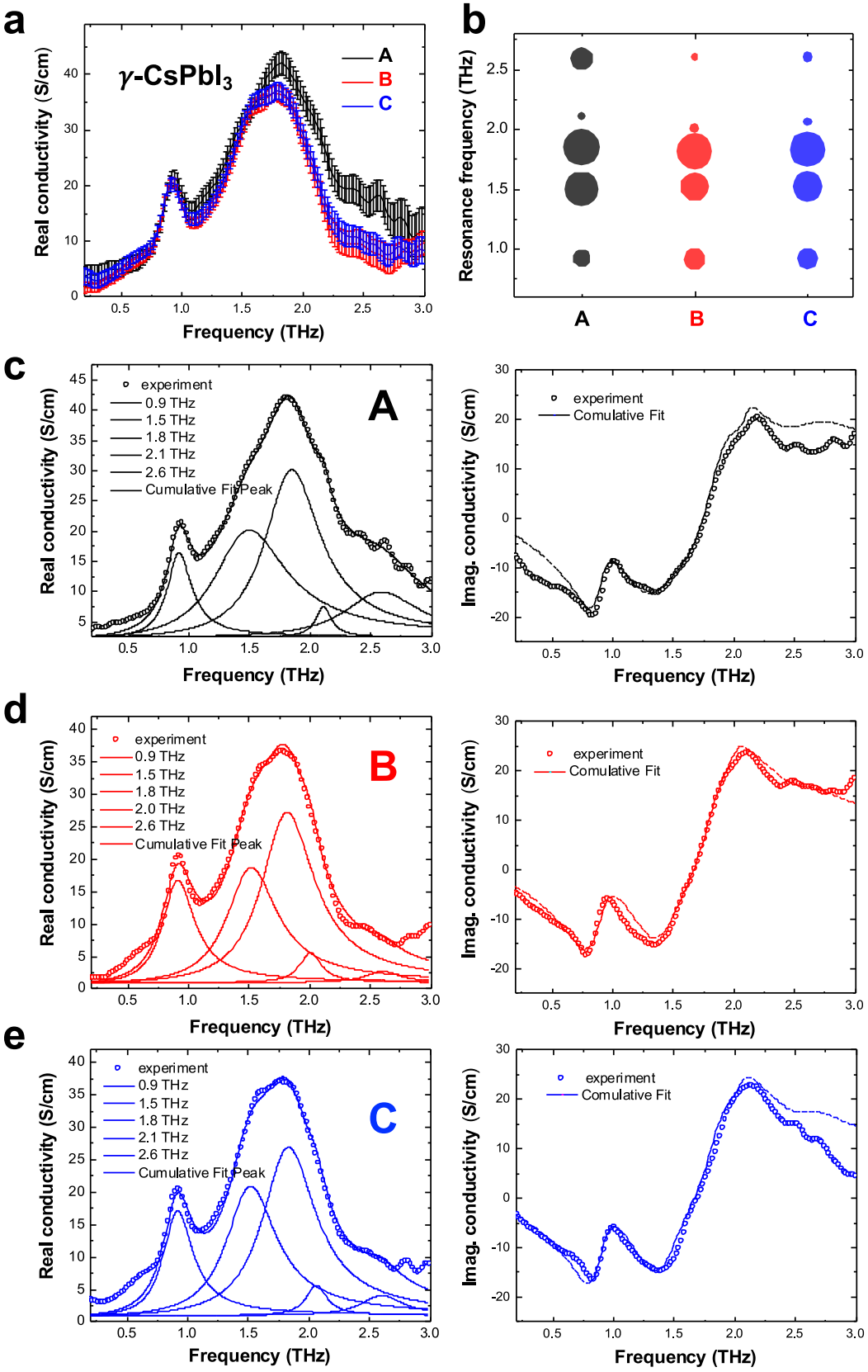

Fig. 3. **a** The grain size dependence of real conductivities of γ-$CsPbI_3$ in the frequency range of 0.2–3 THz **b** Resonance frequency and oscillator strength of the Lorentzian parameter. The size of the dot is proportional to the oscillator strength of the Lorentzian parameter. **c-d** Real conductivities and peak-fitting curves for the resonant phonon modes of A, B and C samples.

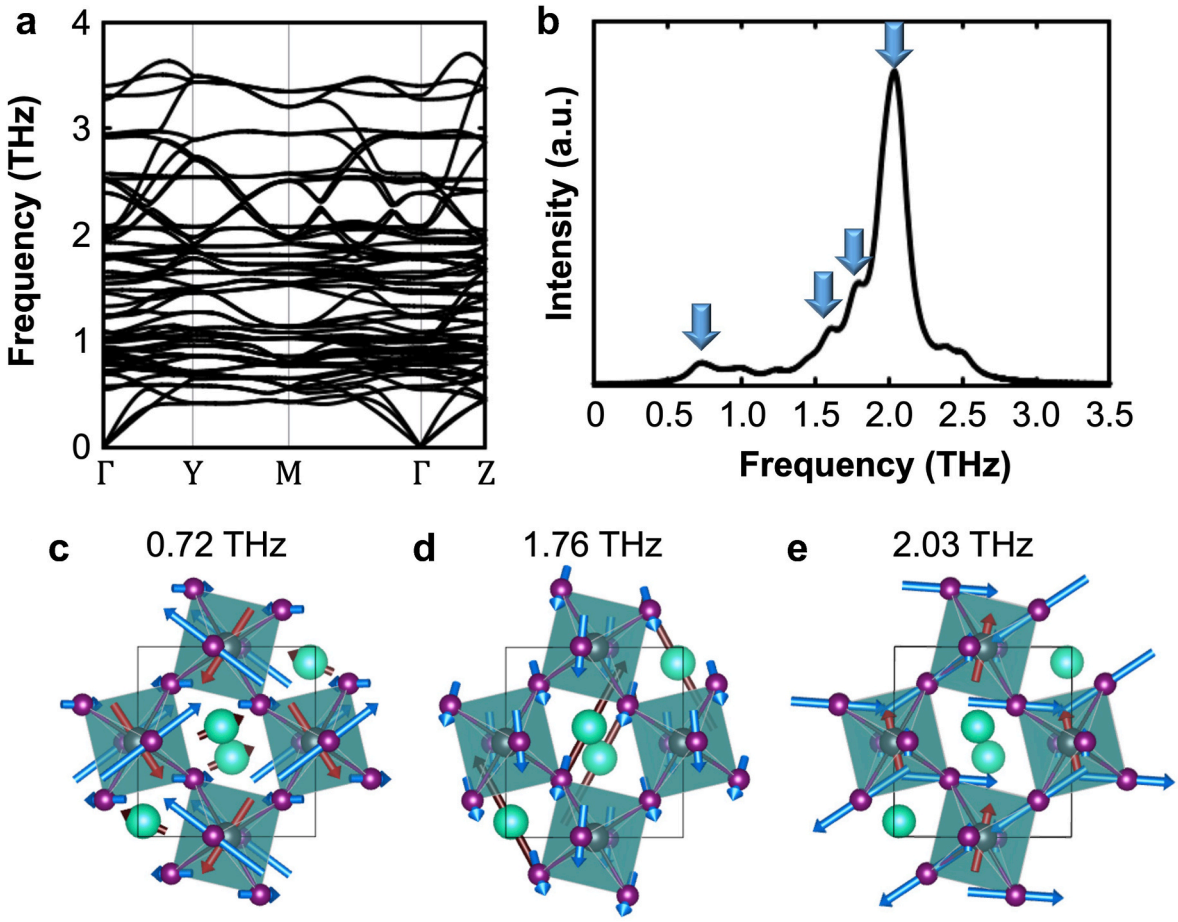

Fig. 4. **a** Phonon band structure and **b** calculated THz absorption spectrum of γ-$CsPbI_3$. **c-e** Real-space visualization of phonon vibration modes of γ-$CsPbI_3$ at 0.72, 1.76, and 2.03 THz. Grey, purple, and cyan balls indicate Pb, I and Cs atoms and red, blue, and brown arrows show their corresponding real-space displacement vectors, respectively. In (b), blue arrows highlight frequencies of the three phonon modes described in **c-e**.

broadening but are also a consequence of intrinsic symmetry.

Following self-degradation, γ-$CsPbI_3$ undergoes a further degradation process and eventually transforms into its δ-phase, which has a THz absorption spectrum that is clearly distinguishable from that of γ-$CsPbI_3$ (Fig. S4). To understand the THz absorption properties of δ-$CsPbI_3$, we calculated its phonon band structures and THz absorption spectra, as shown in Fig. S5 (a) and (b). In the δ phase, the strongest absorption occurs near 1.8 THz, which is a slightly lower frequency than that of the γ phase. In higher-frequency regions, δ-$CsPbI_3$ exhibits a few more absorption peaks in the range of 2.5–3.0 THz, whereas γ-$CsPbI_3$ does not show efficient absorption in that frequency domain. To determine the origin of the phonon modes with the higher frequencies, we represented the real-space atomic vibrations of the main phonon modes of δ-$CsPbI_3$, as shown in Fig. S6. During the phase transition from the γ-to the δ-phase, the octahedral Pb–I structure is broken, and a 1D chain-like Pb–I structure emerges. As a result, δ-$CsPbI_3$ contains quasi-one-dimensional Pb–I chain structures, which are bonded parallel to each other with the help of Cs cations. Consequently, the phonon frequency of the vibration along the 1D chain direction is significantly different from that along the perpendicular directions of the chain. As shown in Figs. S6, the strongest THz absorption feature near 1.8 THz originates from the optical vibration along the chain, whereas the higher-frequency modes correspond to orthogonal vibrational modes. Furthermore, similar to the γ-phase, our calculated THz spectra show very good agreement with the experimentally measured absorption spectrum. These results unambiguously confirm that the observed THz spectra of δ-$CsPbI_3$ originate purely from bulk phonon vibrations and not from the interface or defects.

5. Conclusion

We investigated the phonon vibration modes of all-inorganic perovskite thin films composed of γ-$CsPbI_3$ and determined the integrity at the grain boundary, producing clear evidence that no structural defects that induce defect-incorporated phonon modes. Three major phonon vibration modes were observed at 0.9, 1.5, and 1.8 THz, originating from the transverse I–Pb–I frame, the Cs–I–Cs optical vibration, and the longitudinal I–Pb–I frame, respectively, in good agreement with theoretical simulations. The real conductivity of this all-inorganic perovskite thin film occupied the range of approximately 10–40 S/cm across a broad spectral range of 0.5–3.0 THz, implying attractive potential as a THz detector application. To realize a THz detector using a perovskite material, we strongly recommend using a multilayer technique utilizing both organic-inorganic hybrid and all-inorganic perovskite materials to cover more high real high conductivity and board THz range.

Credit author statement

Inhee Maeng: Investigation, Writing-Original draft preparation, Funding Acquisition Shi Chen: Investigation, Writing-Original draft preparation Seungjin Lee: Software, Formal analysis, Investigation, Writing-Original draft preparation Shenghao Wang: Writing - Reviewing and Editing, Supervision, Funding Acquisition Young-Kyun Kwon: Writing - Reviewing and Editing, Supervision, Funding Acquisition Min-Cherl Jung: Conceptualization, Writing - Reviewing and Editing, Supervision, Project administration, Funding Acquisition.

Declaration of competing interest

The authors declare that they have no known competing financial interests or personal relationships that could have appeared to influence the work reported in this paper.

Data availability

Data will be made available on request.

Acknowledgments

This work was supported by funding from the internal budget of the University of Tsukuba (Japan). This work was also supported by funding from the Program for Professor of Special Appointment (Eastern Scholar) at the Shanghai Institutions of Higher Learning and the Shanghai Rising-Star Program (Grant No. 19QA1403800). This work was further supported by a National Research Foundation of Korea (NRF) grant funded by the Korean government (MSIT) (NRF-2020R1C1C1013646 and NRF-2022R1A2C100550511). A portion of our computational work was performed using the resources of the KISTI Supercomputing Center (KSC-2021-CRE-0479 and KSC-2022-CRE-0062).

Appendix A. Supplementary data

Supplementary data to this article can be found online at https://doi.org/10.1016/j.mtphys.2022.100960.

References

[1] I. Maeng, S. Lee, H. Tanaka, J.H. Yun, S. Wang, M. Nakamura, Y.K. Kwon, M.-C. Jung, Unique phonon modes of a $CH_3NH_3PbBr_3$ hybrid perovskite film without the influence of defect structures: an attempt toward a novel THz-based application, NPG Asia Mater. 12 (2020) 53, https://doi.org/10.1038/s41427-020-0235-6.

[2] I. Maeng, S. Lee, E.Q. Han, Y. Zhang, S.J. Oh, M. Nakamura, J.H. Yun, L. Wang, Y. K. Kwon, M.-C. Jung, Unusual terahertz-wave absorptions in δ/α-mixed-phase FAPbI3 single crystals: interfacial phonon vibration modes, NPG Asia Mater. 13 (2021) 75, https://doi.org/10.1038/s41427-021-00343-7.

[3] Y.M. Lee, J.H. Yun, A. Matsuyama, S. Kobori, I. Maeng, M. Lyu, S. Wang, L. Wang, M.-C. Jung, M. Nakamura, Significant THz-wave absorption property in mixed δ- and α-$FAPbI_3$ hybrid perovskite flexible thin film formed by sequential vacuum evaporation, Appl. Phys. Express 12 (2019): 051003, https://doi.org/10.7567/1882-0786/ab0eec.

[4] I. Maeng, Y.M. Lee, J. Park, S.R. Raga, C. Kang, C.S. Kee, B.D. Yu, S. Hong, L. K. Ono, Y. Qi, M.-C. Jung, M. Nakamura, Significant THz absorption in CH_3NH_2 molecular defect-incorporated organic-inorganic hybrid perovskite thin film, Sci. Rep. 9 (2019) 5811, https://doi.org/10.1038/s41598-019-42359-8.

[5] I. Maeng, A. Matsuyama, J.-H. Yun, S. Wang, C. Kang, C.-S. Kee, M. Nakamura, M.-C. Jung, Strong linear correlation between CH_3NH_2 molecular defect and THz-wave absorption in $CH_3NH_3PbI_3$ hybrid perovskite thin film, Nanomaterials 10 (2020) 721, https://doi.org/10.3390/nano10040721.

[6] E. Cinquanta, D. Meggiolaro, S.G. Motti, M. Gandini, M.J.P. Alcocer, Q. A. Akkerman, C. Vozzi, L. Manna, F. de Angelis, A. Petrozza, S. Stagira, Ultrafast THz probe of photoinduced polarons in lead-halide perovskites, Phys. Rev. Lett. 122 (2019): 166601, https://doi.org/10.1103/PhysRevLett.122.166601.

[7] N.-G. Park, M. Grätzel, T. Miyasaka, Organic-Inorganic Halide Perovskite Photovoltaics from Fundamentals to Device Architectures, Springer, 2016, https://doi.org/10.1007/978-3-319-35114-8.

[8] H. Kim, J. Hunger, E. Cánovas, M. Karakus, Z. Mics, M. Grechko, D. Turchinovich, S.H. Parekh, M. Bonn, Direct observation of mode-specific phonon-band gap coupling in methylammonium lead halide perovskites, Nat. Commun. 8 (2017) 687, https://doi.org/10.1038/s41467-017-00807-x.

[9] M. Sendner, P.K. Nayak, D.A. Egger, S. Beck, C. Müller, B. Epding, W. Kowalsky, L. Kronik, H.J. Snaith, A. Pucci, R. Lovrinčić, Optical phonons in methylammonium lead halide perovskites and implications for charge transport, Mater. Horiz. 3 (2016) 613–620, https://doi.org/10.1039/c6mh00275g.

[10] T. Kohmoto, M. Masui, M. Abe, T. Moriyasu, K. Tanaka, Ultrafast dynamics of soft phonon modes in perovskite dielectrics observed by coherent phonon spectroscopy, Phys. Rev. B Condens. Matter 83 (2011): 064304, https://doi.org/10.1103/PhysRevB.83.064304.

[11] M. Nagai, T. Tomioka, M. Ashida, M. Hoyano, R. Akashi, Y. Yamada, T. Aharen, Y. Kanemitsu, Longitudinal optical phonons modified by organic molecular cation motions in organic-inorganic hybrid perovskites, Phys. Rev. Lett. 121 (2018): 145506, https://doi.org/10.1103/PhysRevLett.121.145506.

[12] A.M.A. Leguy, A.R. Goñi, J.M. Frost, J. Skelton, F. Brivio, X. Rodríguez-Martínez, O.J. Weber, A. Pallipurath, M.I. Alonso, M. Campoy-Quiles, M.T. Weller, J. Nelson, A. Walsh, P.R.F. Barnes, Dynamic disorder, phonon lifetimes, and the assignment of modes to the vibrational spectra of methylammonium lead halide perovskites, Phys. Chem. Chem. Phys. 18 (2016) 27051–27066, https://doi.org/10.1039/c6cp03474h.

[13] D. Zhao, J.M. Skelton, H. Hu, C. La-O-Vorakiat, J.X. Zhu, R.A. Marcus, M.E. Michel-Beyerle, Y.M. Lam, A. Walsh, E.E.M. Chia, Low-frequency optical phonon modes and carrier mobility in the halide perovskite $CH_3NH_3PbBr_3$ using terahertz time-domain spectroscopy, Appl. Phys. Lett. 111 (2017): 201903, https://doi.org/10.1063/1.4993524.

[14] Q. Qiu, Z. Huang, Photodetectors of 2D materials from ultraviolet to terahertz waves, Adv. Mater. 33 (2021): 2008126, https://doi.org/10.1002/adma.202008126.

[15] Y. Xie, F. Liang, S. Chi, D. Wang, K. Zhong, H. Yu, H. Zhang, Y. Chen, J. Wang, Defect engineering of MoS_2 for room-temperature terahertz photodetection, ACS Appl. Mater. Interfaces 12 (2020) 7351–7357, https://doi.org/10.1021/acsami.9b21671.

[16] J. Li, Y. Zou, D. Hu, Y. Gu, Z. Han, J. Liu, X. Xu, Enhanced room-temperature terahertz detection and imaging derived from anti-reflection 2D perovskite layer on $MAPbI_3$ single crystals, Nanoscale 14 (2022) 6109–6117, https://doi.org/10.1039/d2nr00497f.

[17] Y. Li, Y. Zhang, T. Li, M. Li, Z. Chen, Q. Li, H. Zhao, Q. Sheng, W. Shi, J. Yao, Ultrabroadband, ultraviolet to terahertz, and high sensitivity $CH_3NH_3PbI_3$ Perovskite photodetectors, Nano Lett. 20 (2020) 5646–5654, https://doi.org/10.1021/acs.nanolett.0c00082.

[18] R. Montecucco, E. Quadrivi, R. Po, G. Grancini, All-inorganic cesium-based hybrid perovskites for efficient and stable solar cells and modules, Adv. Energy Mater. 11 (2021), https://doi.org/10.1002/aenm.202100672.

[19] Y. Wang, X. Liu, T. Zhang, X. Wang, M. Kan, J. Shi, Y. Zhao, The role of dimethylammonium iodide in $CsPbI_3$ perovskite fabrication: additive or dopant? Angew. Chem. Int. Ed. 58 (2019) 16691–16696, https://doi.org/10.1002/anie.201910800.

[20] A. Marronnier, G. Roma, S. Boyer-Richard, L. Pedesseau, J.M. Jancu, Y. Bonnassieux, C. Katan, C.C. Stoumpos, M.G. Kanatzidis, J. Even, Anharmonicity and disorder in the black phases of cesium lead iodide used for stable inorganic perovskite solar cells, ACS Nano 12 (2018) 3477–3486, https://doi.org/10.1021/acsnano.8b00267.

[21] Y. Wang, M. Ibrahim Dar, L.K. Ono, T. Zhang, M. Kan, Y. Li, L. Zhang, X. Wang, Y. Yang, X. Gao, Y. Qi, M. Grätzel, Y. Zhao, Thermodynamically stabilized b-$CsPbI_3$–based perovskite solar cells with efficiencies >18%, Science 365 (2019) 591–595, https://doi.org/10.1126/science.aav8680.

[22] Z. Liu, L. Qiu, E.J. Juarez-Perez, Z. Hawash, T. Kim, Y. Jiang, Z. Wu, S.R. Raga, L. K. Ono, S. (Frank) Liu, Y. Qi, Gas-solid reaction based over one-micrometer thick stable perovskite films for efficient solar cells and modules, Nat. Commun. 9 (2018) 1–11, https://doi.org/10.1038/s41467-018-06317-8.

[23] H. Choi, S. Kim, I. Maeng, J.-H. Son, H. Park, Improving signal-to-noise ratio of a terahertz signal using a WaveNet-based neural network, Opt. Express 30 (2022) 5473, https://doi.org/10.1364/oe.448279.

[24] W. Kohn, L.J. Sham, Self-consistent Equations Including Exchange and Correlation Effects 140 (1965) A1133, https://doi.org/10.1103/PhysRev.140.A1133.

[25] G. Kresse, J. Furthmüller, Efficient iterative schemes for Ab initio total-energy calculations using a plane-wave basis set, 54, 1996, pp. 11169–11186, https://doi.org/10.1103/PhysRevB.54.11169.

[26] G. Kresse, J. Hafner, Ab initio molecular dynamics for liquid metals, 47 (1993) 558–561, https://doi.org/10.1103/PhysRevB.47.558.

[27] P.E. Blöchl, Projector augmented-wave method, 50 (1994) 17953–17979, https://doi.org/10.1103/PhysRevB.50.17953.

[28] G. Kresse, D. Joubert, From ultrasoft pseudopotentials to the projector augmented-wave method, Phys. Rev. B 59 (1999) 1758–1775, https://doi.org/10.1103/PhysRevB.59.1758.

[29] J.P. Perdew, A. Ruzsinszky, G.I. Csonka, O.A. Vydrov, G.E. Scuseria, L. A. Constantin, X. Zhou, K. Burke, Restoring the density-gradient expansion for exchange in solids and surfaces, Phys. Rev. Lett. 100 (2007): 136406, https://doi.org/10.1103/PhysRevLett.100.136406.

[30] A. Togo, I. Tanaka, First principles phonon calculations in materials science, Scripta Mater. 108 (2015) 1–5, https://doi.org/10.1016/j.scriptamat.2015.07.021.

[31] J.M. Skelton, L.A. Burton, A.J. Jackson, F. Oba, S.C. Parker, A. Walsh, Lattice dynamics of the tin sulphides SnS_2, SnS and Sn_2S_3: vibrational spectra and thermal transport, Phys. Chem. Chem. Phys. 19 (2017) 12452–12465, https://doi.org/10.1039/c7cp01680h.

[32] R. Montecucco, E. Quadrivi, R. Po, G. Grancini, All-inorganic cesium-based hybrid perovskites for efficient and stable solar cells and modules, Adv. Energy Mater. 11 (2021): 2100672, https://doi.org/10.1002/aenm.202100672.

[33] I. Maeng, A. Matsuyama, M. Nakamura, M.-C. Jung, Correlation of THz-wave absorption properties by different halogen elements in FAPb(Br, I)-based hybrid perovskite thin films, Appl. Phys. Express 14 (2021): 121002, https://doi.org/10.35848/1882-0786/ac36b2.

[34] I. Maeng, H. Tanaka, V.K. Mag-usara, M. Nakajima, M. Nakamura, M.C. Jung, Terahertz wave absorption property of all mixed organic–inorganic hybrid perovskite thin film MA(Sn, Pb)(Br, I)$_3$ fabricated by sequential vacuum evaporation method, Front. Chem. 9 (2021): 753141, https://doi.org/10.3389/fchem.2021.753141.

[35] L. Duvillaret, F. Garet, J.L. Coutaz, A reliable method for extraction of material parameters in terahertz time-domain spectroscopy, IEEE J. Sel. Top. Quant. Electron. 2 (1996) 739–745, https://doi.org/10.1109/2944.571775.
[36] C. La-O-Vorakiat, H. Xia, J. Kadro, T. Salim, D. Zhao, T. Ahmed, Y.M. Lam, J. X. Zhu, R.A. Marcus, M.E. Michel-Beyerle, E.E.M. Chia, Phonon mode transformation across the orthohombic-tetragonal phase transition in a lead iodide perovskite $CH_3NH_3PbI_3$: a terahertz time-domain spectroscopy approach, J. Phys. Chem. Lett. 7 (2016) 1–6, https://doi.org/10.1021/acs.jpclett.5b02223.
[37] R.J. Sutton, M.R. Filip, A.A. Haghighirad, N. Sakai, B. Wenger, F. Giustino, H. J. Snaith, Cubic or orthorhombic? Revealing the crystal structure of metastable black-phase CsPbI3 by theory and experiment, ACS Energy Lett. 3 (2018) 1787–1794, https://doi.org/10.1021/acsenergylett.8b00672.